Biogeosciences Discuss., 10, 7171–7200, 2013
www.biogeosciences-discuss.net/10/7171/2013/
doi:10.5194/bgd-10-7171-2013

Biogeosciences Discussions
Open Access

Multiresolution quantification of deciduousness in West Central African forests

G. Viennois[1], N. Barbier[2], I. Fabre[3], and P. Couteron[2]

[1]Centre National de la Recherche Scientifique (CNRS), UMR AMAP, TA A-51/PS 2, Boulevard de la Lironde, Montpellier Cedex5, 34398, France
[2]Institut de Recherche pour le Développement (IRD), UMR AMAP, TA A-51/PS 2, Boulevard de la Lironde, Montpellier Cedex5, 34398, France
[3]Institut Agronomique Néo-Calédonien, Station de Recherche Agronomique de Saint Louis, BP 711, 98810 Mont Dore, New Caledonia, France

Received: 15 February 2013 – Accepted: 4 April 2013 – Published: 23 April 2013

Correspondence to: G. Viennois (gaelle.viennois@cirad.fr)

Published by Copernicus Publications on behalf of the European Geosciences Union.

Abstract

The characterization of leaf phenology in tropical forests is of major importance and improves our understanding of earth-atmosphere-climate interactions. The availability of satellite optical data with a high temporal resolution has permitted the identification of unexpected phenological cycles, particularly over the Amazon region. A primary issue in these studies is the relationship between the optical reflectance of pixels of 1 km or more in size and ground information of limited spatial extent. In this paper, we demonstrate that optical data with high to very-high spatial resolution can help bridge this scale gap by providing snapshots of the canopy that allow discernment of the leaf-phenological stage of trees and the proportions of leaved crowns within the canopy. We also propose applications for broad-scale forest characterization and mapping in West Central Africa over an area of 141 000 km^2.

Eleven years of the Moderate Resolution Imaging Spectroradiometer (MODIS) Enhanced Vegetation Index (EVI) data were averaged over the wet and dry seasons to provide a dataset of optimal radiometric quality at a spatial resolution of 250 m. Sample areas covered at a very-high (GeoEye) and high (SPOT-5) spatial resolution were used to identify forest types and to quantify the proportion of leaved trees in the canopy. The dry season EVI was positively correlated with the proportion of leaved trees in the canopy. This relationship allowed the conversion of EVI into canopy deciduousness at the regional level. On this basis, ecologically important forest types could be mapped, including young secondary, open *Marantaceae*, *Gilbertiodendron dewevrei* and swamp forests. We show that in west central African forests, a large share of the variability in canopy reflectance, as captured by the EVI, is due to variation in the proportion of leaved trees in the upper canopy, thereby opening new perspectives for biodiversity and carbon-cycle applications.

BGD
10, 7171–7200, 2013

1 Introduction

Although tropical forests are now widely accepted as an important component of the global carbon cycle, little is known about the actual dynamics of these ecosystems and on their response to the ever-changing constraints of natural and anthropic inputs at temporal scales ranging from ice age to seasonal cycles (Maley, 2009; Richards, 1996). For example, the monitoring of permanent forest plots in the Amazon and Congo basins suggested an ongoing trend where mortality, growth and recruitment rates changed in coherent patterns over the last few decades (Lewis et al., 2009b). The resulting increase in carbon uptake may explain a significant part of the dynamics observed in atmospheric carbon concentrations (Lewis et al., 2009a). This example illustrates the importance of undertaking large-scale and long-term investigations of these relatively poorly known ecosystems. We will focus here on another fundamental aspect of the rates of gas exchange, leaf phenology, which is understood as a temporal and generally cyclical pattern of biological events (in this case, the development and shedding of leaves) over the seasons. The phenology of rainforest trees is notoriously difficult to study. Multi-annual cycles or cases of partial-leaf shedding within a population or even a single crown are frequent (Richards, 1996). The duration of the leafless stage varies significantly, and some trees have no leafless stage (leaf exchanging). Although the timing of leaf abscission or production is sometimes phased with rainfall cycles, this is not a general case in moist forests, and other drivers, such as episodes of lower incoming radiation (light), may be in play (Wright and Van Schaik, 1994). The apparent complexity of individual behaviors and the lack of synchrony within and among species make it difficult to identify patterns of leaf phenology at the stand or landscape level exclusively on the basis of environmental predictors. Field methods allowing an indirect assessment at these scales include the flux tower (Malhi et al., 1998; Saleska et al., 2003) and litter trap observations (Chave et al., 2008). However, these methods do not allow the direct estimation of the extent and duration of the leafless stage. Indeed, episodes of increased-CO_2 release may be due to increased soil respiration (Saleska

BGD
10, 7171–7200, 2013

et al., 2003), whereas higher leaf-litter fall may be concomitant with new leaf flushes. Quantifying patterns of leaf phenology in the forest canopy in a consistent manner over broad regions serves various purposes, including the quantification of gas and energy transfer with the atmosphere or the inference of species composition and structure.

Recent progress in satellite technologies offers new prospects for the large scale monitoring of leaf phenology using daily optical-satellite records (i.e., Hyper-temporal data, e.g., from Moderate Resolution Imaging Spectroradiometer (MODIS) sensors) through the seasonal dynamics of canopy reflectance and composite vegetation indices and products such as the Enhanced Vegetation Index (EVI) or the Leaf Area product. These radiometric variations are expected to depend on the canopy structure, relative leaf area, leaf age and physiological status (Huete et al., 2002). These variations may also, less desirably, be due to seasonal changes in the atmosphere, such as aerosol concentrations (Asner and Alencar, 2010), or to uncorrected BRDF effects, such as the seasonal variation in sun height. Despite these potential caveats, unexpected temporal patterns have been consistently observed over Amazonian forests. In particular, peaks in vegetation indices (EVI and LAI) occurred in phase with cycles of incoming radiation (Bradley et al., 2011; Brando et al., 2010), suggesting that light could be an important limiting factor.

Here again, scale transfer is an issue because a pixel resolution of 1 km at best is typically employed in such studies to ensure the continuity of the temporal data series in areas of high haze and cloud cover frequency. This is two orders of magnitude greater than the size of the reference plots, typically 1 ha or less, that are used for ground-based verification studies. The growing availability of multiscale/multiresolution remote sensing data now allows us to bridge this scale gap. Indeed, although they do not allow continuous monitoring of the phenological cycle, optical data at higher spatial resolutions provide snapshots of the proportion of deciduous trees in the canopy (Bohlman, 2010).

In this study, we explore the feasibility and meaning of a phenological characterization of tropical forests at regional scale using a multi-sensor approach. We have

BGD
10, 7171–7200, 2013

focused here on a diverse mosaic of forest types straddling the borders of Cameroon, Congo and Gabon, within the Tri_National Dja Odzala Minkebe (TRIDOM) landscape. White (1983) classified this area as being in the Guineo-congolese phytogeographic region. Interestingly, according to several authors (Lebrun and Gilbert, 1954; Letouzey, 1985; Schnell, 1970), the climatic conditions of the area are transitional (delineated by 1600 mm Mean Annual Precipitation, MAP) between primarily evergreen and primarily deciduous forest types. This transition is characterized by a progressive gradient in the density of deciduous trees in the upper canopy rather than a sharp ecotone. Superimposed on the deciduousness gradient is a second gradient of age since perburbation, with a variety of secondary forests of different maturity levels. A number of regional-scale vegetation maps exist for Central Africa. The earliest were based on photointerpretation (Boulvert, 1986; Letouzey, 1985) or classical phytogeographic approaches (White, 1983). Some of these maps were quite detailed, but interpretation required long years of work using subjective methods, making automation and regional comparisons difficult. More recent approaches were based on combinations of satellite optical, LiDAR and/or RADAR (Baccini et al., 2012; Hansen et al., 2008; Mayaux et al., 2004; Saatchi et al., 2011; Verhegghen et al., 2012). Mayaux (2004) and Verhegghen (2012), in particular, used the temporal variation in Spot VEGETATION NDVI data to characterize the phenological signatures of different ecosystems across Africa with a 1 km resolution. However, apart from very large swamps, young secondary forests or montane forests, none of these recent large-scale maps has allowed precise distinctions to be made between the different types of dense forests observed on the ground in intermingled patchworks, with sometimes sharp and sometimes progressive transitions between each other, forming patterns at both the landscape and the region scale. Compared to previous works that have used medium-resolution optical data (i.e. 100 m to 1 km resolution) for tropical forest mapping and canopy reflectance monitoring, the novelty of our approach is threefold. (1) We maintained an optimal spatial resolution of 250 m for the hyper-temporal data by aggregating eleven years of MODIS terra EVI data over the two main seasons. (2) We used high- (10 m resolution)

BGD
10, 7171–7200, 2013

and very-high-resolution (0.5 m resolution) data to bridge the scale gap between the stand and MODIS pixel levels and thus reached a quantitative interpretation of the EVI variations in terms of the proportion of leaved trees during the dry season. (3) We distinguished and mapped several dense-forest types based on this quantitative phenological proxy.

2 Material

2.1 Study site

The study area covers approximately 141 000 km^2 of the NW edge of the Congo basin at the borders between the Republic of Congo, Gabon and Cameroon. This area broadly covers the Dja-Odzala-Minkébé (Tridom) Landscape (COMIFAC Tridom intergovernmental collaboration agreement, 2005), of which approximately 25 % is protected, including seven national parks and one fauna reserve. Geomorphologically, the area sits on a hilly plateau ranging between 300 and 1000 m above sea level, with localized inselberg outcrops. Proximity to the equator induces a bimodal rainfall regime, with two dry seasons centered in January (main season) and July (small season), totaling four to five dry months, and two wet seasons centered in October and April. Mean annual precipitation ranges from 1600 in the east to 2000 mm in the west. These climatic conditions create a transition from mostly evergreen to mostly deciduous forest types (Lebrun and Gilbert, 1954; Letouzey, 1985; Schnell, 1970). At one extreme of the deciduous gradient stand evergreen forests dominated by *Caesalpiniaceae*. *Gilbertiodendron dewevrei* dominated patches are a peculiar case in these forests. Although strikingly mono-dominant evergreen forests are nearly ubiquitous in the center of the Congo basin, they reach the limit of their distribution in the study area, which may partly explain why they mostly occupy lower topographic positions (Letouzey, 1968). At the other extreme are forests dominated by *Cannabaceae* (ex. *Ulmaceae, Celtis* spp.) and *Malvaceae* (ex. *Sterculiaceae*, e.g., *Cola* spp.), for which deciduous trees make

BGD
10, 7171–7200, 2013

up to 70 % of the upper canopy (Lebrun and Gilbert, 1954). Superimposed on this deciduousness gradient is a second gradient of age since perturbation, with a variety of secondary forests of different maturity levels. In the temporal succession, *Musanga cecropioides* is the first tree species to close the canopy. This fast-growing pioneer is progressively outgrown by hemi-heliophilous trees, such as *Triplochiton scleroxylon, Alstonia Boonei* and *Terminalia superba* (Schnell, 1970). These latter trees are mostly deciduous, adding to the complexity of forest classification. The older secondary forests can, in some cases, remain in the succession process for a long period of time when the proliferation of *Marantaceae* lianas develops in the undergrowth, alone or in combination with the activity of large mammals, blocking the regeneration of trees (De Foresta and Massimba, 1990; Letouzey, 1968). These latter forests present a striking gap in the vertical forest stratification, with only scattered tall trees (hence the name open forests) rising to 40 m or so in height and surrounded by the liana layer, which is only a few meters high. Swamp forests typically have various densities of *Uappaca paludosa* trees, with their characteristic stilt roots, and *Raphia* palms. In the NW, stands of *Sterculia violacea* are more dominant in swamp forests. At the southern end of the study area lies the northernmost extent of the Bateke savannas and Kalahari sands.

2.2 Imagery

Hyper-temporal information on canopy reflectance was obtained from the MOD13Q1 product (collection 5) of the Moderate Resolution Imaging Spectroradiometer (MODIS). This product is composited every 16 days at a spatial resolution of 250 m and includes the Red (0.62–0.37 µm), NIR (0.841–0.876 µm), Blue (0.459–0.479 µm) and MIR (1.23–1.25 µm) spectral bands as well as the derived "enhanced" vegetation index, or EVI. The EVI (EVI = 2.5 (NIR – Red)/(NIR + 6 Red – 7.5 Blue + 1); Gao et al., 2000) optimizes the vegetation signal with improved sensitivity in high biomass regions and reduces atmospheric influences, whereas MIR reflectance from a closed vegetation canopy is determined primarily by canopy water content (Boyd and Petitcolin, 2004). The study area is covered by the tile h19v08 and has a ground area of

BGD
10, 7171–7200, 2013

250 000 km^2. We downloaded all available dates for this tile between January 2000 and December 2011. In spite of atmospheric corrections, the presence of almost permanent clouds and haze largely corrupted the data. To generate a good quality composite at a 250 m resolution, we aggregated eleven years of valid data (after filtering for pixel reliability and quality using layers provided with the product) for the EVI index and middle-infrared reflectance (MIR) for both the principal dry season (15 November–15 February, months with less than 100 mm rainfall, consistent with Aragao et al., 2007) and wet season (15 February–15 November). This approach is an important simplification, that neglects both inter-annual variations in dry season length or severity and the existence of a shorter and less intense dry season centered on July. However obtaining a coherent dataset required finding a compromise between the spatial and the temporal resolution, and we chose here to sacrifice the latter (e.g. as opposed to Bradley et al., 2011). We thus obtained aggregated EVI and MIR images for the wet season and for the main dry season.

We obtained 25 archive SPOT-5 ©CNES images at pre-treatment level 1b (High Resolution, HR) for the main dry season from the CNES-ISIS program. Two particularly cloud and haze-free dry season images (lat 5.14/long 12.97 and lat 3.51/long 16.02) were chosen within this dataset to calibrate quantitative relationships between leafiness and EVI variations. Each image covered an area close to 4000 km^2. These images had a pixel size of 10 m and were composed of four spectral bands: Green (0.5–0.59 µm), Red (0.61–0.68 µm), NIR band (0.78–0.89 µm) and MIR band (1.58–1.75 µm).

Four very-high-resolution (VHR) main-dry-season images (GeoEye) were acquired within areas covered by the SPOT-5 image dataset. Each image covers an area of the study area close to 100 km^2. The sensor spatial resolution of the multispectral bands (2 m) was improved using a Brovey Pansharpening algorithm (Vrabel, 1996), resulting in a final pixel size of 0.5 m. Each image is composed of four spectral bands: Blue (0.45–0.51 µm), Green (0.51–0.58 µm), Red (0.655–0.69 µm) and NIR (0.78–0.92 µm).

All images were orthorectified and referenced against the Landsat GeoCover mosaic (Tucker et al., 2004) and SRTM topography (Farr et al., 2007) products. Both HR

BGD
10, 7171–7200, 2013

and THR images were visually analyzed as color (R-G-B) composites of the Red-NIR-Green bands.

3 Methods

3.1 Mapping of forest types

Reference areas were delimited by visual interpretation of pansharpened GeoEye (VHR) images. With a spatial resolution of 0.5 m, these images allowed the discernment of forest structural types (Fig. 1) on the basis of general canopy patterns (texture) (Barbier et al., 2010; Couteron et al., 2005) to the level of individual tree crowns (Clark et al., 2005). In addition, the multi-spectral information allowed the discernment of leaved vs. deciduous crowns, which is of paramount importance for this study. It is worth noting that photointerpretation has a long tradition in forestry, including in our study area, where Letouzey (1985) mapped forest types using aerial photography (1 : 50 000). To expand the training areas, we made use of the intermediate scale offered by the SPOT imagery set. On these HR images, the main forest types were still distinguishable through radiometric variations that could be locally interpreted in relation to the VHR imagery (Fig. 1), but were not reliable enough for large-scale mapping given the numerous (atmospheric, instrumental etc.) sources of radiometric instability. The reference areas obtained were used in a maximum-likelihood, supervised classification applied to the MODIS EVI and MIR (wet season and dry season) composite bands, with the aim to segment broad qualitative forest types over the whole study area, based on both the radiometry and its temporal variation.

3.2 Quantifying leafiness

Deciduous and leaved trees are clearly distinguishable on both VHR and HR images (Fig. 1a and b). In both images, the deciduous crowns are distinguishable mainly because they have high Red reflectance and low NIR reflectance. In the GeoEye images,

BGD
10, 7171–7200, 2013

one can clearly distinguish bare branches and twigs (Fig. 1a), whereas in SPOT-5 images, bare crowns are only visible as patches a few pixels wide with high reflectance in the Red band and low response in the NIR band (appearing in pink on the composites presented in Fig. 1b). This spectral property allows deciduous versus leaved trees to be distinguished at multiple spatial scales. A simple, local, radiometric thresholding of the SPOT-5 images was therefore used for the segmentation of the leaved vs. deciduous crowns (see Fig. A1). However, radiometric corrections were crucial to insure the consistency of spectral responses within and between images. Large patches of haze, particularly noticeable in the Red band, were removed via a high pass Fourier filter (Niblack, 1986). Radiometric histograms were then aligned between the images by standardization around the mean, under the assumption that forest images had globally similar radiometric amplitude. To separate leaved vs. leafless pixels, threshold values in the Red and NIR bands were carefully selected for each SPOT-5 image using the VHR GeoEye data as a visual reference. Binary masks were thus created and leaved SPOT-5 pixels were counted within areas corresponding to the MODIS 250 m pixels.

We used regression to compare the proportion of leaved pixels on SPOT-5 images taken in the dry season against aggregated (2011) dry season EVI values. These calculations were used to calibrate a linear-inversion rule for the prediction of forest deciduousness over the whole study area.

4 Results

4.1 Forest segmentation

Photointerpretation on Red-NIR-Green, very-high-resolution (GeoEye) composites allowed a visual discrimination of forest types having contrasting characteristics (Fig. 1). On SPOT-5 composites at a 10 m spatial resolution, differences between forest types were still locally detectable as subtle spectral variations (Fig. 1). This fact allowed the creation of reference polygons over sufficient areas to be scaled up to the MODIS level.

BGD
10, 7171–7200, 2013

In more detail, Mixed forests (MF1–4) appeared as a mixture of pinkish, large, bare crowns and branches of emergent deciduous trees and green leaved crowns of other broad-leaved trees, without obvious signs of degradation (Fig. 1a and b). MF were separable from the other types, but less so among themselves, due to the continuous variation in the proportion of leafless crowns.

Open forests (OF) were composed of Marantaceae forests with large trees interspersed within a light-green, highly photosynthetic matrix of tall herbs and vines (Fig. 1c and d). Tree crowns may in some case form a nearly closed cover, but most often, they let the *Marantaceae* carpet appear, conditioning a texture characterized by both fine- (undergrowth) and coarse- (isolated crowns) grained patterns on GeoEye imagery (Fig. 1c). Appearance of the undergrowth also tends to produce high reflectance levels in the NIR, producing green patches in the SPOT composites (Fig. 1d). Young secondary forests (YSF) in the early post-disturbance stages showed fine-grained texture on GeoEye composites (Fig. 1e). *Musanga cecropioides* trees tended to form a uniform cover with very high NIR reflectance values (Fig. 1f), while deciduous trees were generally absent. Monodominant *Gilbertiodendron dewevrei* forests (GDF1–2) presented a typical fine-grained texture, due to the even-size and high-density distribution of canopy trees (Fig. 1g and h). Deciduous trees appeared only occasionally. Possibly in relation to low leaf reflectance and pendulous-angle distribution of the dominant species, global reflectances in NIR and Red were surprisingly low, as indicated by dark tones on the GeoEye and SPOT composites and by low EVI values in both MODIS seasonal coverages. Swamp forests (SF), were easily recognizable on GeoEye images by the dominance of *Raphia* spp. palms with a characteristic star-shaped appearance. In dry season images, *Raphia* trees presented low NIR and high Red reflectances, making them appear leafless, but MIR values were also characteristically low (see Fig. A2).

A maximum-likelihood supervised classification was applied to the EVI and MIR wet season and dry season composite images on the basis of the references polygons. Although differences between forest classes are significant in the EVI, separability

BGD
10, 7171–7200, 2013

(measured using the Jeffries-Matusita Distance, Richards, 1999) was improved by including MIR dry and wet season aggregated images. This was particularly important to discriminate swamp forests, as MIR values are significantly lower than any other class, especially in the dry season (Table 1, Fig. A2).

We extracted the spectral signatures of each forest class in the EVI dry season and wet season aggregated images. The distribution of wet- and dry-season mean EVI values within each forest class is depicted in Fig. 2 with summary distribution statistics (boxplots). Importantly and as expected, mean dry season EVI values were always lower than mean wet season values for all forest types (Fig. 2). A two-factor (season + forest class) analysis of variance was significant ($p < 0.0001$) for both factors tested and for their interaction. Basic assumptions of normality and homoscedasticity were verified. Inter-class and inter-season differences of the mean EVI values were tested using a Newman-Keuls multi-comparison test. All classes and seasons showed very significant differences ($p < 0.0001$) between each other, except for the MF2/MF1 and MF3/MF4 pairs (see Table 1), which were not significantly different in Wet Season. Overall, three broad groups stood out (Fig. 2). The first group contained swamp forests (SF) and monodominant *Gilbertiodendron dewevrei* forests (GDF1 and GDF2) and presented low mean EVI values throughout the two seasons. On the other hand, the group containing open Marantaceae forests (OF) and young secondary forests (YSF) displayed consistently high mean EVI values. The mixed forests (MF1 to MF4) formed a third group presenting intermediate EVI values with noticeable interclass differences in annual variability. Indeed, EVI distributions became increasingly bimodal (i.e. showing higher difference between the dry and wet season values) from MF1 to MF4, suggesting varying degrees of deciduousness.

4.2 Quantifying and predicting leafiness

To illustrate the relationship between the phenological characterizations performed using high-resolution SPOT-5 images and the MODIS mean EVI values, Fig. 3 maps the spatial patterns in the proportion of leaved pixels and mean EVI values for the dry

BGD
10, 7171–7200, 2013

and wet seasons. For each season, these two patterns co-varied in space. The EVI and proportion of leaved pixels varied spatially and temporally in the same way. More quantitatively, a good correlation was obtained between the proportion of leaved pixels estimated form SPOT-5 dry season images (2011) and mean EVI values averaged over the single 2011 dry season (Fig. 2, $n = 43\,498$, $R^2 = 0.55$, p value < 0.05, major axis regression: $y = 0.1649x + 0.26$). Slightly different values were obtained when using dry season EVI values averaged for the 2000–2011 period ($n = 43\,498$, $R^2 = 0.48$, p value < 0.05, major axis regression: $y = 0.1290x + 0.30$). However, because of the longer averaged period, the latter EVI composite layer proved more stable in terms of radiometric quality (absence of obvious discontinuities) over the study area.

We therefore used the 2000–2011 regression coefficients and EVI composite layer to perform a linear inversion of leafiness values over the entire study area. The resulting map, shown in Fig. 5, combined qualitative information for the YSF, OF, GDF, and SF classes and for other non-forest land-cover classes, as well as the values of the quantitative leafiness variable within the MF class. The map presents a very coherent spatial structure, with degraded forest types (YSF, OF) primarily located near inhabited localities and road networks, GDF and SF forming localized pockets in lower topographic positions, and dry season leafiness values varying over broad regions. Additionally, the most deciduous forests (lower-leafiness values) were primarily located in the driest eastern part of the study area.

5 Discussion

Our results show that the mean, dry-season EVI is linearly and positively correlated with the proportion of leaved trees in the canopy, as can be assessed using high- and very-high-spatial-resolution images. This correlation provides strong evidence that a large share of the variability in canopy reflectance summarized in the EVI at stand level (250 m pixels) in the mixed forests (MF) of west central Africa is due to variation in the proportion of leaved trees in the upper canopy. In our study area, mixed forests

BGD
10, 7171–7200, 2013

displayed the broadest extent and also the largest inter-annual variations in EVI. In addition, our approach allowed mapping of ecologically important forest types that presented consistently high (young secondary forests and open Marantaceae Forests) or consistently low EVI values (*Gilbertiodendron dewevrei* forests and swamp forests). Another important result concerning the influence of climate drivers is that in all of the forest types identified, the lowest EVI values were observed during the main dry season. This element contrasts with findings from other tropical forests, notably in the Amazon basin, where different relationships between climate and EVI variation were reported. Indeed, over large areas of the Amazon region, the EVI peaked in the dry season, in phase with higher incoming light periods (Brando et al., 2010; Huete et al., 2006; Myneni et al., 2007). However, the dry season is generally very cloudy over West Central Africa (Riou, 1984). Therefore, incoming light levels are higher in the wet season. In other words, it is difficult on correlative grounds to decide whether water or light was the main climatic driver or limiting factor for our study area. It is possible however, that both water and light reach their least limiting levels during the main wet season. In any case, the multi-resolution approach presented here could be easily applied to different contexts, thereby enabling comparisons.

The share of EVI variation that remained unexplained by leafiness values may have come from a number of different sources, including the imperfect temporal match between the data sources. HR and VHR images were opportunistic snapshots through the clouds, whereas a consistent coverage of MODIS data required aggregating data over long periods of time. Additionally, the radiometric (e.g., atmospheric, Bidirectional Reflectance Distribution Function – BRDF) corrections performed over the different datasets were imperfect. For instance, the sun height is not accounted for in MODIS data filtering algorithms (Vermote et al., 2002) despite the fact that this factor varies seasonally and does influence the BRDF. However, systematic "in phase" variations between sun height and EVI were not evident in preliminary tests we made over different areas, including the Amazon basin (results not shown). Last but not least, other biological sources of variation in canopy reflectance may have been in play, such as

BGD
10, 7171–7200, 2013

variations in canopy structure, leaf age, and flowering and fruiting episodes (Borchert, 1996; van Schaik et al., 1993).

Considering all of these error sources and the known complexity in leaf phenology within and among tree species in tropical forests (Reich, 1995), the correlation obtained between leafiness values and EVI is surprisingly good and consistent with Bohlman (2010). This correlation is very much in line with the coherent regional patterns displayed by the seasonal variations of the EVI. This suggests that stand-level leaf-phenology signatures do indeed exist at large scales, indicating some degree of synchrony in tree phenology (Borchert et al., 2002; van Schaik et al., 1993).

The spatial distribution of leafiness values and of the various forest types we mapped was largely consistent with existing detailed or phytogeographic vegetation maps for the region we studied (Letouzey, 1968; White, 1983). Indeed, we found a gradient in the density of deciduous trees in the upper canopy of mixed forests that decreased from the north west to the south east of the study area, as has been suggested by several authors (Lebrun and Gilbert, 1954; Letouzey, 1985; White, 1983). Degraded forest types (YSF, OF) were primarily located near inhabited localities and road networks. *Gilbertiodendron dewevrei* forests were often located in confined pockets in lower topographic positions of the south east of Cameroon, as was observed by Letouzey (1968). Landscape-scale variations, in the form of intermingled mosaics, corresponded to complex biological (i.e., variations in species abundance), environmental substratum conditions (Gourlet-Fleury et al., 2011), and historically numerous, ancient settlements (Cinnamon, 2003). A comparison of our map with the reference map of Mayaux (2004) (See Fig. A3) illustrates the important gain in detail regarding the discrimination of forest types. The purpose and scale of these maps is different, as the latter map covers the entire continent. However, in Mayaux's map, all mixed deciduous forests types, as well as open Marantaceae forests, were grouped under unit 40 or "Closed to open broadleaved evergreen or semi-deciduous forest". *Gilbertiodendron* monodominant stands, on the other hand, were grouped with swamp forests and open water/marshes within unit 160 or "Closed to open broadleaved forest regularly flooded".

BGD
10, 7171–7200, 2013

A quick comparison (not shown) with the benchmark biomass map of Saatchi (Saatchi et al., 2011) showed a generally lower biomass ($< 150\,\mathrm{Mg\,DM\,ha^{-1}}$) in areas dominated by open Marantaceae forests (e.g., in the Congolese region). However, pockets of *Gilbertiodendron* forests, which should present significantly higher biomass levels (Djuikouo et al., 2010), did not show up on the benchmark map.

Numerous field visits performed by some of these authors also provided information for data validation. However, a systematic/statistical analysis of the correspondence between floristic gradients and phenology patterns would require very large datasets that have not yet been gathered. Forest-management inventories could prove useful in this regard (Gond, 2012; Gourlet-Fleury et al., 2011; Maniatis et al., 2011). Another important path that needs to be explored further is the modeling of radiative transfer in 3-D, forest-stand models (Barbier et al., 2011, 2012; Gastellu-Etchegorry, 2008). Even with the crude parameterization of forest structure and surface/volume scattering properties, such models have proven their usefulness for detecting both instrumental and biological sources of variability and perturbation (Barbier et al., 2011). After long-lasting controversy over the possible meaning and caveats of reflectance variations in Amazon canopies (Huete and Saleska, 2010; Samanta et al., 2011), these new research tracks offer exciting opportunities to bridge the scale gap between field observation and large-scale, remotely sensed patterns that are accessible through MODIS imagery. A more rigorous large-scale, quantitative characterization of canopy phenology opens exiting potential for the parameterization of more realistic, dynamic global vegetation models (Bonan, 2008), or for, more generally, the strategic monitoring of forest cover in tropical countries.

Acknowledgements. Spot images where acquired in the framework of the *SPOT/Programme ISIS, Copyright CNES*. This research is part of the pilot regional program (PPR) "Global changes biodiversity and health in the tropical wet forests of Central Africa" of the IRD and has benefited from the support of various partner institutions and researchers. We are especially grateful to Bonaventure Sonké, Vincent Droissart, and Pierre Ploton for sharing their field experience and helping us to interpret our results.

BGD
10, 7171–7200, 2013

References

Aragão, L. E. O., Malhi, Y., Roman-Cuesta, R. M., Saatchi, S., Anderson, L. O., and Shimabukuro, Y. E.: Spatial patterns and fire response of recent Amazonian droughts, Geophys. Res. Lett., 34, L07701, doi:10.1029/2006GL028946, 2007.

Asner, G. P. and Alencar, A.: Drought impacts on the Amazon forest: the remote sensing perspective, New Phytol., 187, 569–578, 2010.

Baccini, A., Goetz, S. J., Walker, W. S., Laporte, N. T., Sun, M., Sulla-Menashe, D., Hackler, J., Beck, P. S. A., Dubayah, R., and Friedl, M. A.: Estimated carbon dioxide emissions from tropical deforestation improved by carbon-density maps, Nat. Clim. Change, 2, 182–185, 2012.

Barbier, N., Couteron, P., Proisy, C., Malhi, Y., and Gastellu-Etchegorry, J.-P.: The variation of apparent crown size and canopy heterogeneity across lowland Amazonian forests, Global. Ecol. Biogeogr., 19, 72–84, 2010.

Barbier, N., Proisy, C., Véga, C., Sabatier, D., and Couteron, P.: Bidirectional texture function of high resolution optical images of tropical forest: an approach using LiDAR hillshade simulations, Remote Sens. Environ., 115, 167–179, 2011.

Barbier, N., Couteron, P., Gastelly-Etchegorry, J. P., and Proisy, C.: Linking canopy images to forest structural parameters: potential of a modeling framework, Ann. For. Sci., 69, 305–311, 2012.

Bohlman, S. A.: Landscape patterns and environmental controls of deciduousness in forests of central Panama, Global. Ecol. Biogeogr., 19, 376–385, 2010.

Bonan, G. B.: Forests and climate change: forcings, feedbacks, and the climate benefits of forests, Science, 320, 1444–1449, 2008.

Borchert, R.: Phenology and flowering periodicity of Neotropical dry forest species: evidence from herbarium collections, J. Trop. Ecol., 12, 65–80, 1996.

Borchert, R., Rivera, G., and Hagnauer, W.: Modification of vegetative phenology in a tropical semi-deciduous forest by abnormal drought and rain, Biotropica, 34, 27–39, 2002.

Boulvert, Y.: Carte phytogéographique de la République Centrafricaine (feuille Ouest-feuille Est) à 1 : 1 000 000, 1986.

Boyd, D. S. and Petitcolin, F.: Remote sensing of the terrestrial environment using middle infrared radiation (3.0–5.0 µm), Int. J. Remote Sens., 25, 3343–3368, 2004.

BGD
10, 7171–7200, 2013

Bradley, A. V., Gerard, F. F., Barbier, N., Weedon, G. P., Anderson, L. O., Huntingford, C., Aragao, L. E. O. C., Zelazowski, P., and Arai, E.: Relationships between phenology, radiation and precipitation in the Amazon region, Glob. Change Biol., 17, 2245–2260, 2011.

Brando, P. M., Goetz, S. J., Baccini, A., Nepstad, D. C., Beck, P. S. A., and Christman, M. C.: Seasonal and interannual variability of climate and vegetation indices across the Amazon, P. Natl. Acad. Sci. USA, 107, 14685–14690, 2010.

Chave, J., Condit, R., Muller-Landau, H. C., Thomas., S. C., Ashton, P. S., Bunyavejchewin, S., Dattaraja, H. S., Davies, S. J., Esufali, S., Ewango, C. E. N., Feeley, K. J., Foster, R. B., Gunatilleke, N., Gunatilleke, S., Hall, P., Hart, T. B., Hernández, C., Hubbell, S. P., Itoh, A., Kiratiprayoon, S., LaFrankie, J. V., de Lao, S. L., Makana, J. R., Supardi Noor, M. N., Kassim, A. R., Samper, C., Sukumar, R., Suresh, H. S., Tan, S., Thompson, J., Tongco, M. D. C., Valencia, R., Vallejo, M., Villa, G., Yamakura, T., Zimmerman, J. K., and Losos, E. C.: Assessing evidence for a pervasive alteration in tropical tree communities, PLoS Biol., 6, e45, doi:10.1371/journal.pbio.0060045, 2008.

Cinnamon, J.: Narrating equatorial African landscapes: conservation, histories, and endangered forests in northern Gabon, J. Colonial. Colonial Hist., 4, Project MUSE, 2003.

Clark, M. L., Roberts, D. A., and Clark, D. B.: Hyperspectral discrimination of tropical rain forest tree species at leaf to crown scales, Remote Sens. Environ., 96, 375–398, 2005.

Couteron, P., Pelissier, R., Nicolini, E. A. and Paget, D.: Predicting tropical forest stand structure parameters from Fourier transform of very high-resolution remotely sensed canopy images, J. Appl. Ecol., 42, 1121–1128, 2005.

Djuikouo, M. N. K., Doucet, J. L., Nguembou, C. K., Lewis, S. L., and Sonké, B.: Diversity and aboveground biomass in three tropical forest types in the Dja Biosphere Reserve, Cameroon, Afr. J. Ecol., 48, 1053–1063, 2010.

Farr, T. G., Rosen, P. A., Caro, E., Crippen, R., Duren, R., Hensley, S., Kobrick, M., Paller, M., Rodriguez, E., Roth, L., Seal, D., Shaffer, S., Shimada, J., Umland J., Werner, M., Oskin, M., Burbank, D., and Alsdorf, D.: The shuttle radar topography mission, Reviews of Geophysics–Richmond Virginia then Washington, 45, RG2004, doi:10.1029/2005RG000183, 2007.

De Foresta, H. and Massimba, J. P.: Etude descriptive d'une forêt clairsemée à Marantaceae dans le Mayombe Congolais, ORSTOM, Raymond Lanfranchi et Dominique Schwartz, 1990.

Gao, X., Huete, A. R., Ni, W., and Miura, T.: Optical-biophysical relationships of vegetation spectra without background contamination, Remote Sens. Environ., 74, 609–620, 2000.

BGD
10, 7171–7200, 2013

Gastellu-Etchegorry, J. P.: 3-D modeling of satellite spectral images, radiation budget and energy budget of urban landscapes, Meteorol. Atmos. Phys., 102, 187–207, 2008.
Gond, V.: Climatic control on the structure and functioning or the moist forest in the Congo Basin, Climate Change Deforestation and the Future of African Rainforests, International Conference, Oxford, UK, 4 January, 2012.
Gourlet-Fleury, S., Rossi, V., Rejou-Mechain, M., Freycon, V., Fayolle, A., Saint-André, L., Cornu, G., Gerard, J., Sarrailh, J. M., and Flores, O.: Environmental filtering of dense-wooded species controls above-ground biomass stored in African moist forests, J. Ecol., 99, 981–990, 2011.
Hansen, M. C., Roy, D. P., Lindquist, E., Adusei, B., Justice, C. O. and Altstatt, A.: A method for integrating MODIS and Landsat data for systematic monitoring of forest cover and change in the Congo Basin, Remote Sens. Environ., 112, 2495–2513, 2008.
Huete, A., Didan, K., Miura, T., Rodriguez, E. P., Gao, X., and Ferreira, L. G.: Overview of the radiometric and biophysical performance of the MODIS vegetation indices, Remote Sens. Environ., 83, 195–213, 2002.
Huete, A. R., Didan, K., Shimabukuro, Y. E., Ratana, P., Saleska, S. R., Hutyra, L. R., Yang, W., Nemani, R. R. and Myneni, R.: Amazon rainforests green-up with sunlight in dry season, Geophys. Res. Lett., 33, L06405, doi:10.1029/2005GL025583, 2006.
Huete, A. R. and Saleska, S. R.: Remote sensing of tropical forest phenology: issues and controversies, ISRPS J. Photogramm., 23, 539–541, 2010.
Lebrun, J. and Gilbert, G.: Une classification écologique des forêts du congo, Série scientifique N° 63., edited by P. de l'institut national pour l'étude agronomique du congo belge, 1954.
Letouzey, R.: Etude phytogéographique du Cameroun, Lechevalier, Paris, France, 1968.
Letouzey, R.: Notice de la carte phytogeographique du Cameroun au 1 : 500 000 (1985): 2, M-SM: region afro-montagnarde et etage submontagnard, 27, 1985.
Lewis, S. L., Lloyd, J., Sitch, S., Mitchard, E. T. A., and Laurance, W. F.: Changing ecology of tropical forests: evidence and drivers, Ann. Rev. Ecol. Evol. S., 40, 529–549, 2009a.
Lewis, S. L., Lopez-Gonzalez, G., Sonké, B., Affum-Baffoe, K., Baker, T. R., Ojo, L. O., Phillips, O. L., Reitsma, J. M., White, L., Comiskey, J. A. K, Djuikouo, M. N., Ewango, C. E. N., Feldpausch, T. R., Hamilton, A. C., Gloor, M., Hart, T., Hladik, A., Lloyd, J., Lovett, J. C., Makana, J. R., Malhi, Y., Mbago, F. M., Ndangalasi, H. J., Peacock, J., Peh, K. S. H., Sheil, D., Sunderland, T., Swaine, M. D., Taplin, J., Taylor, D., Thomas, S. C., Votere, R., and Wöll, H.: Increasing carbon storage in intact African tropical forests, Nature, 457, 1003–1006, 2009b.

BGD
10, 7171–7200, 2013

Maley, J.: A catastrophic destruction of African forests about 2,500 years ago still exerts a major influence on present vegetation formations, IDS bulletin, 33, 13–30, 2009.
Malhi, Y., Nobre, A. D., Grace, J., Kruijt, B., Pereira, M. G. P., Culf, A., and Scott, S.: Carbon dioxide transfer over a Central Amazonian rain forest, J. Geophys. Res., 103, 593–31, 1998.
Maniatis, D., Malhi, Y., Saint André, L., Mollicone, D., Barbier, N., Saatchi, S., Henry, M., Tellier, L., Schwartzenberg, M., and White, L.: Evaluating the Potential of Commercial Forest Inventory Data to Report on Forest Carbon Stock and Forest Carbon Stock Changes for REDD, Int. J. Forest. Res., Article ID 134526, 13 pp., doi:10.1155/2011/134526, 2011.
Mayaux, P., Bartholomé, E., Fritz, S., and Belward, A.: A new land-cover map of Africa for the year 2000, J. Biogeogr., 31, 861–877, 2004.
Myneni, R. B., Yang, W., Nemani, R. R., Huete, A. R., Dickinson, R. E., Knyazikhin, Y., Didan, K., Fu, R., Negron Juarez, R. I., Saatchi, S. S., Hashimoto, H., Ichii, K., Shabanov, N. V., Tan, B., Ratana, P., Privette, J. L., Morisette, J. T., Vermote, E. F., Roy, D. P., Wolfe, R. E., Friedl, M. A., Running, S. W., Votava, P., El-Saleous, N., Devadiga, S., Su, Y., and Salomonson, V. V. : Large seasonal swings in leaf area of Amazon rainforests, P. Natl. Acad. Sci. USA, 104, 4820–4823, 2007.
Niblack, W.: An introduction to digital image processing, Prentice-Hall International, 1986.
Reich, P. B.: Phenology of tropical forests: patterns, causes, and consequences, Can. J. Bot., 73, 164–174, 1995.
Richards, J. A.: Remote Sensing Digital Image Analysis: An Introduction, Springer-Verlag, Berlin, 1999.
Richards, P. W.: The Tropical Rainforest, Cambridge, 1996.
Riou, C.: Experimental study of potential evapotranspiration (PET) in Central Africa, J. Hydrol., 72, 275–288, 1984.
Saatchi, S. S., Harris, N. L., Brown, S., Lefsky, M., Mitchard, E. T. A., Salas, W., Zutta, B. R., Buermann, W., Lewis, S. L., and Hagen, S.: Benchmark map of forest carbon stocks in tropical regions across three continents, P. Natl. Acad. Sci. USA, 108, 9899–9904, 2011.
Saleska, S. R., Miller, S. D., Matross, D. M., Goulden, M. L., Wofsy, S. C., Da Rocha, H. R., De Camargo, P. B., Crill, P., Daube, B. C., De Freitas, H. C., Hutyra, L., Keller, M., Kirchhoff, V., Menton, M., Munger, W., Pyle, E. H., Rice, A. H., and Silva H.: Carbon in Amazon forests: unexpected seasonal fluxes and disturbance-induced losses, Science, 302, 1554–1557, 2003.
Samanta, A., Ganguly, S., and Myneni, R. B.: MODIS enhanced vegetation index data do not show greening of Amazon forests during the 2005 drought, New Phytol., 189, 11–15, 2011.

BGD
10, 7171–7200, 2013

Schnell, R.: Introduction a la Phytogeographie des Pays Tropicaux, V.3., 1970.
Tucker, C. J., Grant, D. M., and Dykstra, J. D.: NASA's global orthorectified Landsat data set, Photogramm. Eng. Rem. S., 70, 313–322, 2004.
Van Schaik, C. P., Terborgh, J. W., and Wright, S. J.: The phenology of tropical forests: adaptive significance and consequences for primary consumers, Ann. Rev. Ecol. Syst., 24, 353–377, 1993.
Verhegghen, A., Mayaux, P., de Wasseige, C., and Defourny, P.: Mapping Congo Basin vegetation types from 300 m and 1 km multi-sensor time series for carbon stocks and forest areas estimation, Biogeosciences, 9, 5061–5079, doi:10.5194/bg-9-5061-2012, 2012.
Vermote, E. F., El Saleous, N. Z., and Justice, C. O.: Atmospheric correction of MODIS data in the visible to middle infrared: first results, Remote Sens. Environ., 83, 97–111, 2002.
Vrabel, J.: Multispectral imagery band sharpening study, Photogramm. Eng. Rem. S., 62, 1075–1084, 1996.
White, F. The vegetation of Africa: a descriptive memoir to accompany the UNESCO/AEFTAT/UNSO Vegetation Map of Africa, UNESCO, Paris, 1983.
Wright, S. J. and Van Schaik, C. P.: Light and the phenology of tropical trees, Am. Naturalist, 143, 192–199, 1994.

BGD
10, 7171–7200, 2013

Table 1. Newman-Keuls multi-comparison test after two-factor (season + class) analysis of variance of EVI and MIR.

Forest class	Season	N	Mean EVI	Std. Err	EVI Group	Mean MIR	Std. Err	MIR Group
GDF1	DS	354	3693	5.95	B	481	0.93	C
GDF1	WS	354	4604	6.47	K	527	0.89	G
GDF2	DS	501	3756	6.07	C	467	0.95	B
GDF2	WS	501	4236	6.50	G	517	1.12	F
MF1	DS	742	4272	3.57	H	493	0.63	D
MF1	WS	742	4651	3.45	L	496	0.79	D
MF2	DS	766	3911	3.45	E	483	1.66	C
MF2	WS	766	4644	3.37	L	518	1.20	E–F
MF3	DS	211	4200	6.62	F	578	3.82	J
MF3	WS	211	4951	6.48	N	559	1.60	I
MF4	DS	440	3831	4.84	D	509	0.95	E
MF4	WS	440	4958	5.51	N	552	1.18	I
OF	DS	211	4473	8.46	J	535	3.39	G–H
OF	WS	292	5338	8.55	P	596	3.62	K
SF	DS	70	3538	15.81	A	419	3.78	A
SF	WS	70	4384	15.07	I	472	2.83	B
YSF	DS	380	4709	8.68	M	540	2.41	H
YSF	WS	380	5309	9.16	O	580	2.33	J

Abbreviations: GDF: monodominant *Gilbertiodendron dewevrei* forests; MF: mixed forest; OF: open forest; YSF: young secondary forest; SF: swamp forest; DS: dry season; WS: wet season.

BGD
10, 7171–7200, 2013

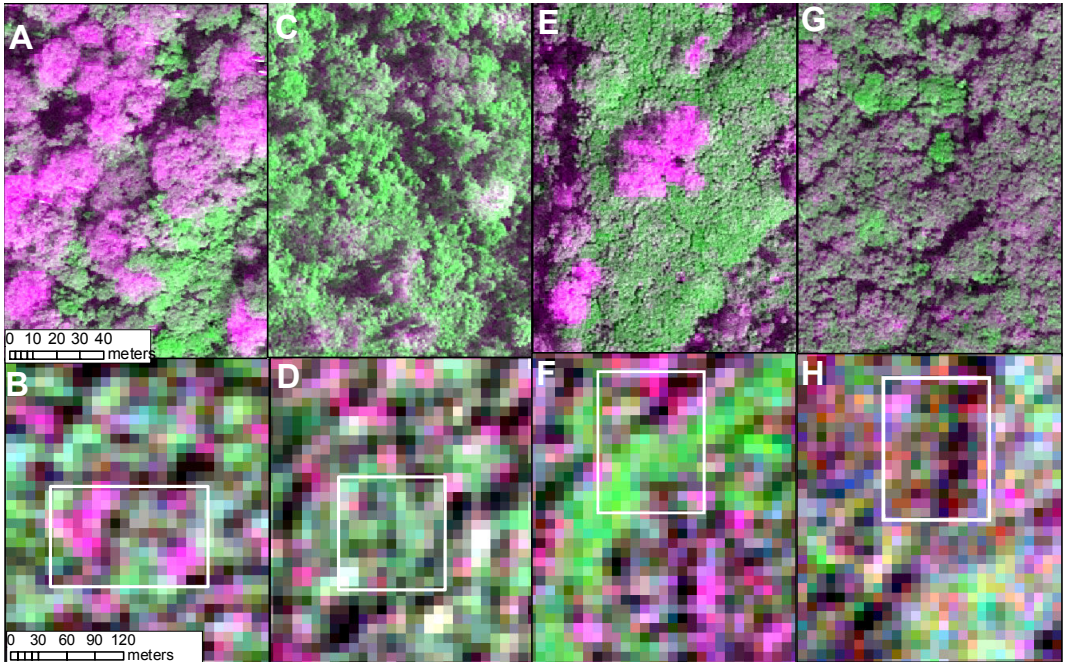

Fig. 1. Characteristics and criteria for visual discrimination of the main forest types on Red-Near Infrared-Green very-high-spatial-resolution GeoEye and high-spatial-resolution SPOT-5 composites acquired in Dry Season. **(A, C, E, G)**: extracts very-high-spatial-resolution GeoEye image (0.5 m pixels). **(B, D, F, H)**: extracts high-spatial-resolution SPOT-5 image (10 m pixels). Footprint of the corresponding GeoEye image appears in the form of white rectangle. (**A** and **B**): mixed forests (MF 1–4); (**C** and **D**): open Marantaceae Forests; (**E** and **F**): young secondary forest; (**G** and **H**): monodominant *Gilbertiodendron dewevrei* forests.

BGD
10, 7171–7200, 2013

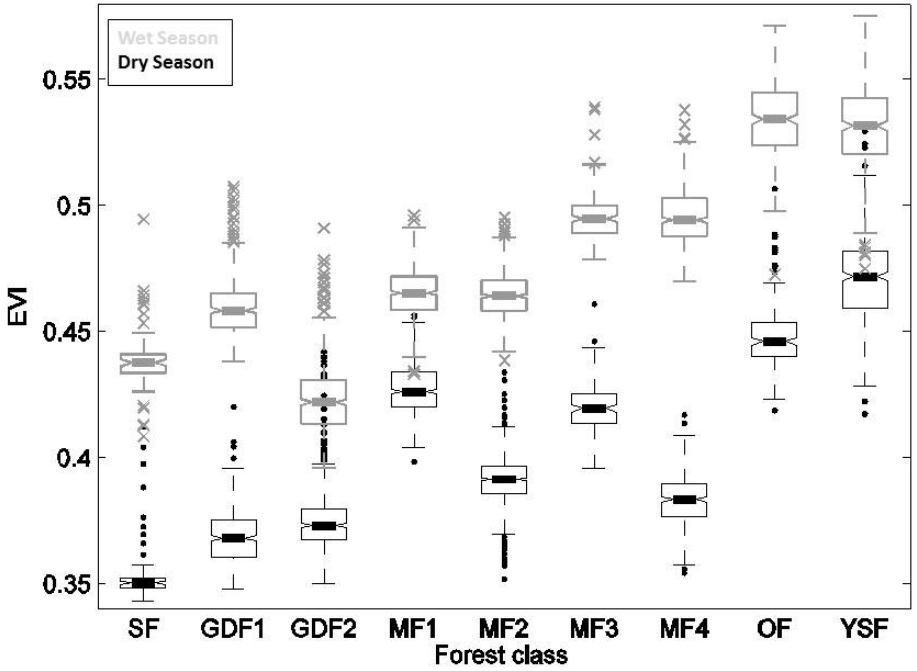

Fig. 2. Distributions of EVI values for the different forest classes. Box-plots summarize EVI values aggregated between 2000 and 2011 for each (wet and dry) season. Two-factor (season + class) analysis of variance of EVI test rejected the null-hypothesis of equality-of-mean EVI values for all the types of forests and seasons ($p < 0.0001$). See also Table 1. Abbreviations: GDF (1–2): monodominant *Gilbertiodendron dewevrei* forests; MF (1–4): mixed forest; OF: open forest; YSF: young secondary forest; SF: swamp forest.

BGD
10, 7171–7200, 2013

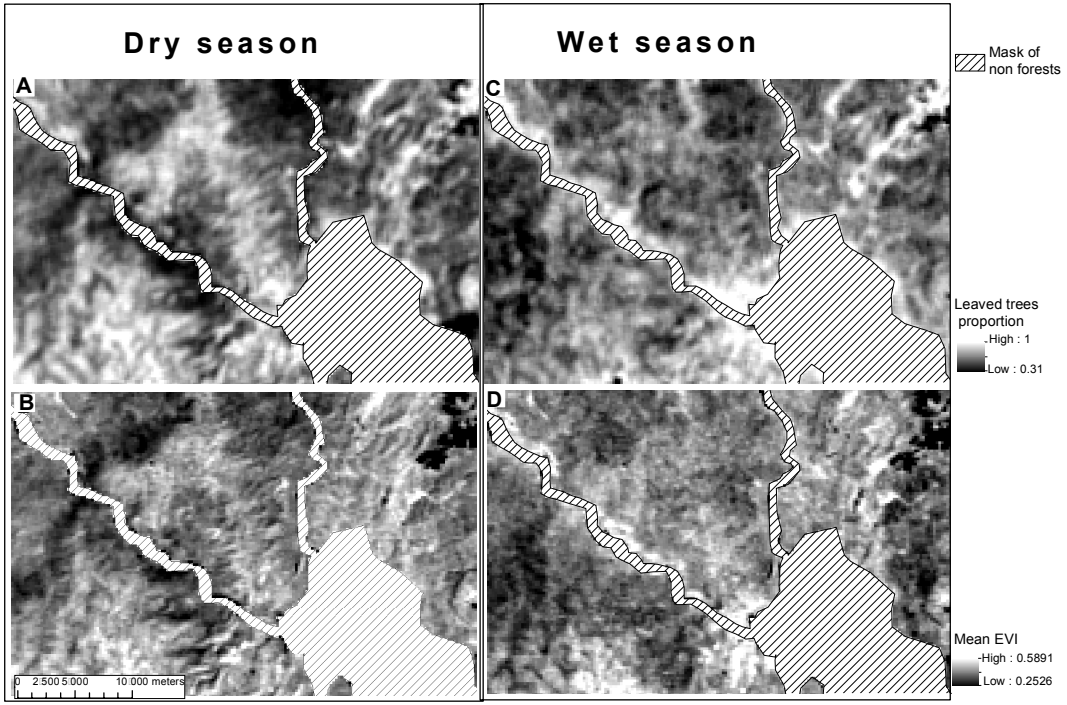

Fig. 3. Maps of the proportion of fully- or partially-leaved trees vs. mean EVI values averaged for either the dry or the wet season. (**A** and **B**): maps of the proportion of leaved trees **(A)** and mean EVI values averaged **(B)** for dry season. (**B** and **D**): maps of the proportion of leaved trees **(C)** and mean EVI values averaged **(D)** for wet season. Masked areas are non-forests.

BGD
10, 7171–7200, 2013

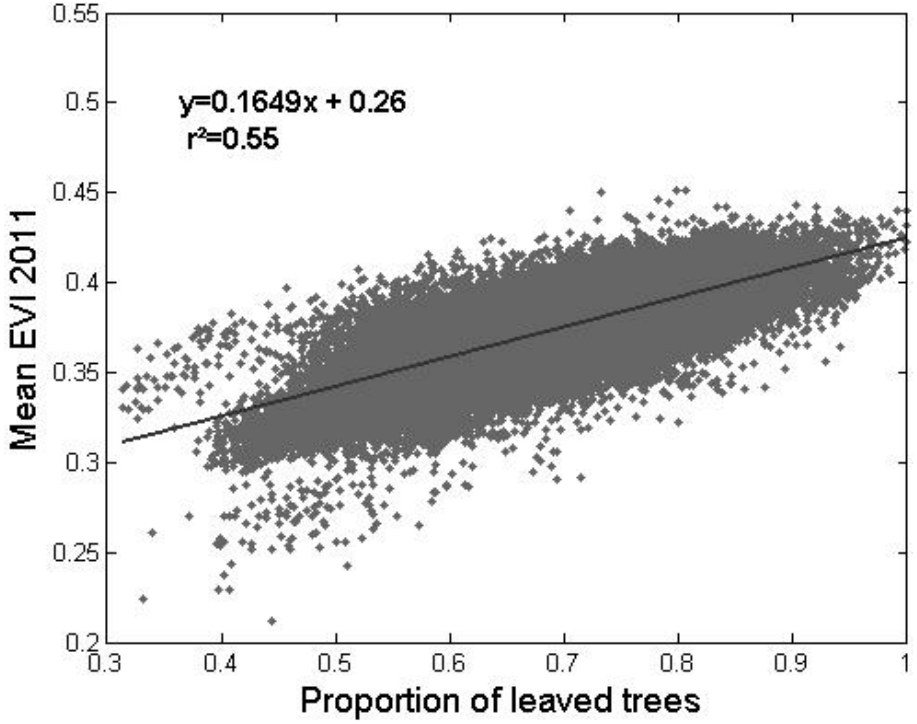

Fig. 4. Linear regression between the proportion of leaved trees and mean EVI values averaged for the dry season of 2011. X-axis: proportion of leaved trees calculated for two different SPOT-5 images acquired in January of 2011 (dry season). Y-axis: mean EVI values for the dry season of the year 2011. The analysis is performed at the resolution of the MODIS product (250 m).

BGD
10, 7171–7200, 2013

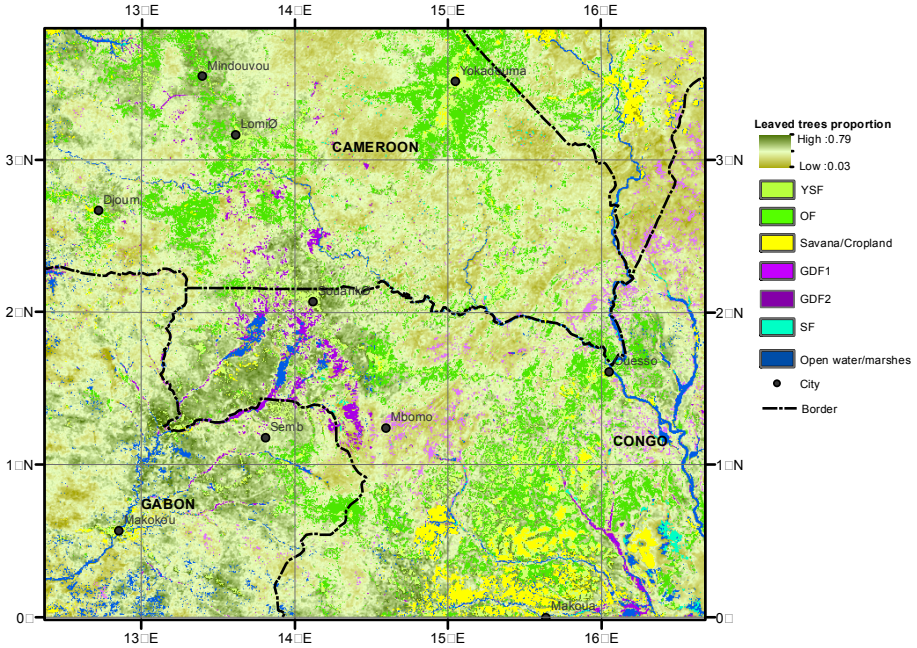

Fig. 5. Map of the distribution of the main forest classes (open forest, young secondary forest, swamp forest and monodominant *Gilbertiodendron dewevrei* forests) along with the MODIS-predicted leaved trees proportion within the mixed forest class, (Map Projection WGS84). The entire map was derived from remotely sensed MODIS pixels of 250 m (aggregation of dry season values). The leaved tree proportion within the MF class was predicted by linear inversion of the leafiness equation: $y = 0.1290x + 0.3$, where Y is dry season EVI values averaged over the 2000–2011 period and x the proportion of leaved trees counted on SPOT 5 images. Abbreviations: GDF (1–2): monodominant *Gilbertiodendron dewevrei* forests; OF: open forest; YSF: young secondary forest; SF: swamp forest.

BGD
10, 7171–7200, 2013

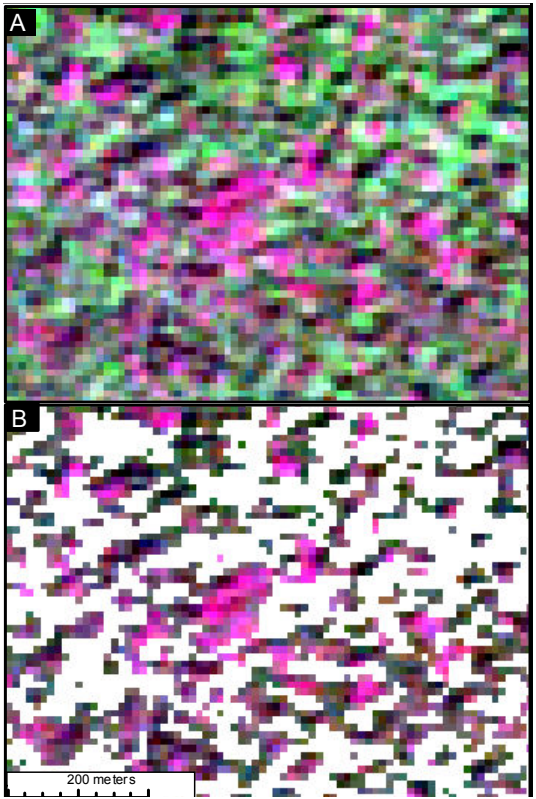

Fig. A1. Thresholding on Red-Near infrared-Green high resolution (SPOT-5) to isolate deciduous trees. **(A)**: in SPOT-5 images, bare crowns of mixed forest appear as patches a few pixels wide with high reflectance in the Red band and low response in the NIR (appearing in pink). **(B)**: thresholding on the Red and NIR bands were applied to SPOT-5 images to isolate the deciduous trees of a mixed forest.

BGD
10, 7171–7200, 2013

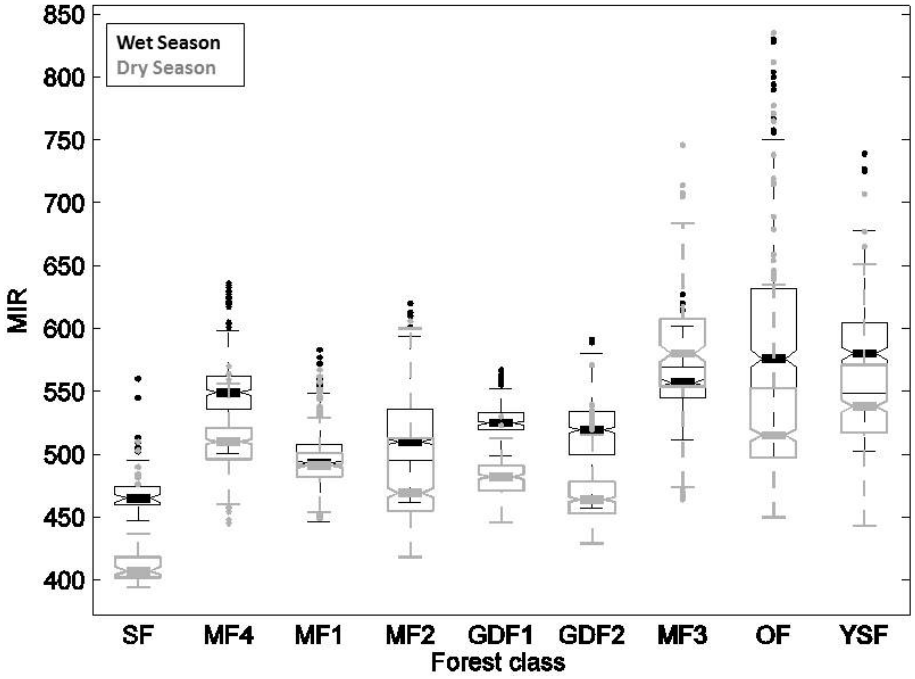

Fig. A2. Distributions of MIR values for the different forest classes. Box-plots summarize the MIR values aggregated between 2000 and 2011 for each wet and dry seasons.

BGD
10, 7171–7200, 2013

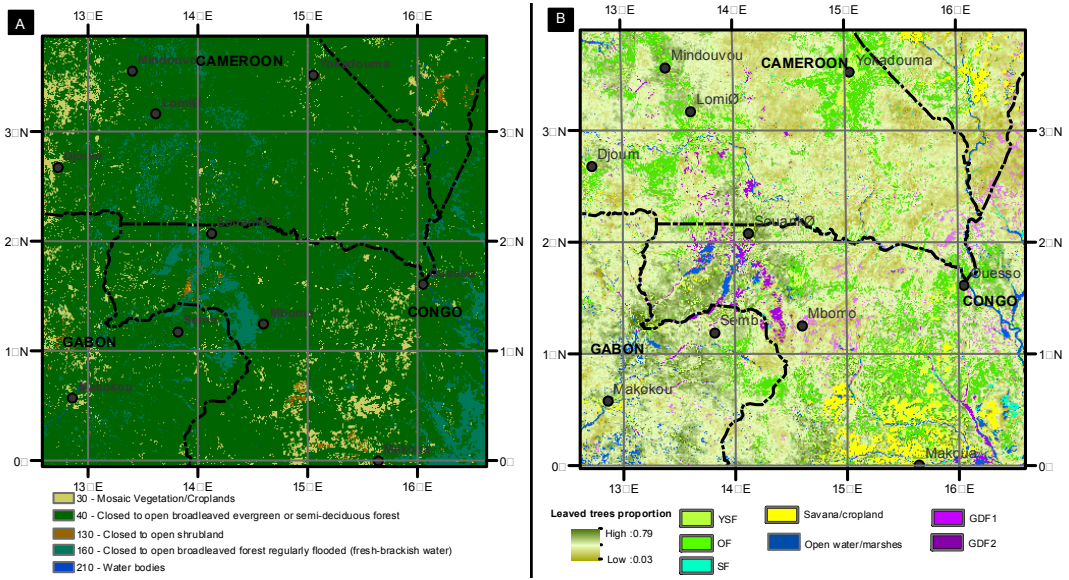

Fig. A3. Comparison of the forest types mapped in this study **(B)** with the land cover map of Africa produced at a spatial resolution of 1 km **(A)** by Mayaux et al. (2004). Abbreviations: GDF (1–2): monodominant *Gilbertiodendron dewevrei* forests; OF: open forest; YSF: young secondary forest; SF: swamp forest.

BGD
10, 7171–7200, 2013